NANO LETTERS

pubs.acs.org/NanoLett

Letter

Giant Valley-Polarized Rydberg Excitons in Monolayer WSe_2 Revealed by Magneto-photocurrent Spectroscopy

Tianmeng Wang,◆ Zhipeng Li,◆ Yunmei Li,◆ Zhengguang Lu,◆ Shengnan Miao, Zhen Lian, Yuze Meng, Mark Blei, Takashi Taniguchi, Kenji Watanabe, Sefaattin Tongay, Dmitry Smirnov, Chuanwei Zhang, and Su-Fei Shi*

Cite This: *Nano Lett.* 2020, 20, 7635−7641

Read Online

ACCESS | Metrics & More | Article Recommendations | Supporting Information

ABSTRACT: A strong Coulomb interaction could lead to a strongly bound exciton with high-order excited states, similar to the Rydberg atom. The interaction of giant Rydberg excitons can be engineered for a correlated ordered exciton array with a Rydberg blockade, which is promising for realizing quantum simulation. Monolayer transition metal dichalcogenides, with their greatly enhanced Coulomb interaction, are an ideal platform to host the Rydberg excitons in two dimensions. Here, we employ helicity-resolved magneto-photocurrent spectroscopy to identify Rydberg exciton states up to 11s in monolayer WSe_2. Notably, the radius of the Rydberg exciton at 11s can be as large as 214 nm, orders of magnitude larger than the 1s exciton. The giant valley-polarized Rydberg exciton not only provides an exciting platform to study the strong exciton−exciton interaction and nonlinear exciton response but also allows the investigation of the different interplay between the Coulomb interaction and Landau quantization, tunable from a low- to high-magnetic-field limit.

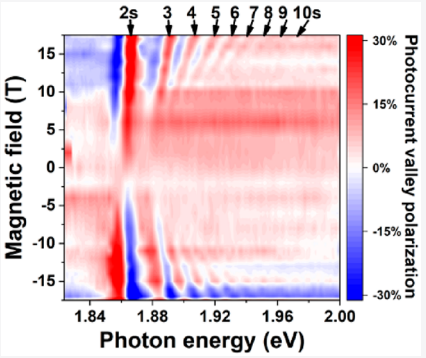

KEYWORDS: *Strong Coulomb interaction, Rydberg exciton, photocurrent spectroscopy, 11s exciton, valley polarization, Landau quantization*

Downloaded via FLORIDA STATE UNIV on March 2, 2026 at 18:51:10 (UTC).
See https://pubs.acs.org/sharingguidelines for options on how to legitimately share published articles.

I. INTRODUCTION

The Rydberg atom,[1−5] with its large size of hundreds of nanometers, can be easily controlled and probed with light. As a result, the Rydberg atom can be used to generate artificial molecules to study molecular dynamics.[6] The giant size of Rydberg atoms also results in an enhanced interaction that leads to large nonlinearity and an exciton Coulomb blockade, which can be utilized for quantum information processing and quantum simulation.[7,8] Despite the significant experimental progress for creating a Rydberg atom in optical traps, its analogue in a solid-state system is still highly desirable for better integration into modern electronic technology. The exciton, a ubiquitous quasiparticle in optically excited semiconductors, consists of a negatively charged electron and a positively charged hole bound together through a Coulomb interaction.[3−5] In bulk semiconductors, excitons would also have Rydberg series like the hydrogen atom, which has been identified by the serial absorption peaks below the bandgap with energy spacing matching the Rydberg description $E_b = -\frac{R_y}{n^2}$, where E_b is the binding energy, R_y is the Rydberg constant, and n is the principal quantum number.[9−12] For large principal number n, the corresponding Rydberg exciton would have a large radius extension and thus strongly enhanced exciton−exciton interaction, which is critical for realizing the large optical nonlinearity needed for quantum optoelectronics. One such example is the Rybderg blockade that can be utilized for quantum computing and quantum sensing,[1−5] in which the exsitence of a large size Rydberg exciton will exclude the possibility of another Rydberg exciton nearby. The Rydberg exciton blockade has been shown for an $n = 25$ exciton found in the crystal of copper oxide (Cu_2O),[9] which has a corresponding Bohr radius of 1.04 μm.

The ordered array of Rydberg excitons can be utilized as a quantum simulator[3] and for quantum computing[7] as well. However, generating such an ordered array in a bulk semiconductor is extremely challenging, if feasible at all. The emergence of the monolayer transition metal dichalcogenides (TMDCs) provides a promising platform to address the challenge.[13] The strongly enhanced Coulomb interaction in two dimensions leads to a robust exciton with a large binding energy, which renders the highly excited state of the exciton possible. The two-dimensional (2D) nature of the TMDCs allows them to be patterned with periodic potential to form an

Received: August 1, 2020
Revised: September 5, 2020
Published: September 9, 2020

ACS Publications

© 2020 American Chemical Society

https://dx.doi.org/10.1021/acs.nanolett.0c03167
Nano Lett. 2020, 20, 7635−7641

ordered array of Rydberg excitons. Also, the valley degrees of freedom of the exciton brings additional control of the Rydberg exciton. Nevertheless, the existence of a giant Rydberg exciton with a size comparable to the optical wavelength remains elusive. So far, only an excited exciton state up to 5s has been revealed in TMDCs,[14] which requires an extremely strong magnetic field (~91 T)[14] and is still too small for convenient optical readout. Does a higher-order Rydberg exciton with a size comparable to an optical wavelength exist in TMDCs at all? That is the central question we want to address in this work.

Here, we employ a helicity-resolved magneto-photocurrent spectroscopy technique to reveal the exciton excited states up to 11s in a high-quality WSe_2 monolayer device under an ~17 T magnetic field, which, to the best of our knowledge, is the highest excited state of exciton ever reported for any 2D semiconductor. Under an out-of-plane magnetic field, the energy degeneracy of the K and K′ valleys is lifted, which can be exploited to improve the signal-to-noise ratio further. The extensive information about the size and energy of the Rydberg series of the exciton, from 1s to 11s, is in excellent agreement with numerical simulations using the non-hydrogenic screened Keldysh potential. Being able to resolve the highly excited state up to 11s, we can accurately determine the exciton binding energy of the A exciton (1s) in WSe_2 to be 168.6 meV, consistent with previous reports.[4,15−18] Notably, the size of the 11s exciton is determined to be 214 nm, orders of magnitude larger than that of the ground-state exciton (1.75 nm for the 1s state, see Table 1) and comparable to the wavelength of light, especially with the consideration of the dielectric environment. The unveiling of the valley-polarized giant Rydberg excitons in monolayer WSe_2 would enable further investigation of the enhanced exciton−exciton interactions. In addition, the 2 orders of magnitude difference of the binding energy between different Rydberg excitons allows the investigation of the interplay between the Coulomb interaction and Landau quantization, which transitions from a low- to high-magnetic-field limit for increasing n. It is worth noting that the high-magnetic-field limit can be reached at a reasonable magnetic field of ~10 T for $n \geq 9$, owing to the small binding energy of the high-order Rydberg exciton (Table 1).

Table 1. Binding Energy and Radius for Each Rydberg Exciton State at B = 0 T, Obtained by Fitting the Experimental Data with the Numerical Calculations

excited states	binding energy (meV)	radius (nm) $r_{ns} = \sqrt{\langle r^2 \rangle_{ns}}$
1s	168.6	1.75
2s	40.0	6.80
3s	17.4	15.45
4s	9.7	27.68
5s	6.1	43.51
6s	4.2	62.94
7s	3.1	85.96
8s	2.4	112.6
9s	1.9	142.9
10s	1.5	176.7
11s	1.2	214.0

The boron nitride (BN) encapsulated monolayer WSe_2 device was fabricated through the method described previously,[19−21] and the schematic is shown in Figure 1a. Two pieces of few-layer graphene were used as the source and drain electrodes of the WSe_2 layer, and one piece of few-layer graphene was used as the top gate electrode, gating the monolayer WSe_2 through the top BN layer. The microscope image of the device is shown in Figure 1b.

The conductance of the WSe_2 device, without light illumination, was measured as a function of the top gate voltage at both room temperature and 4.2 K, as shown in Figure 1c. It is evident that the WSe_2 device exhibits bipolar behaviors and is charge neutral at the gate voltage of 0 V. We then performed spatially resolved photocurrent measurement at 77 K with zero bias voltage applied, by scanning a focused laser spot (~2 μm) across the sample, and measured the resulting photocurrent response as a function of the spatial location of the laser spot. As shown in Figure 1d, it is clear that the photocurrent response at zero bias is mainly from the junction of the few-layer graphene electrode and the monolayer WSe_2, with a photoresponsivity as large as 4.4 μA/W, with the continuous wave (CW) photoexcitation centered at 1.959 eV and an excitation power of 1 μW.

II. RYDBERG EXCITON REVEALED BY MAGNETO-PHOTOCURRENT SPECTROSCOPY

Photocurrent is a sensitive probe of the absorption information on a 2D semiconductor with a large signal-to-noise ratio, due to the large photocurrent response and negligible dark current.[17,22−24] Here, we investigate the photocurrent response from the monolayer WSe_2 device as a function of the excitation photon energy. We also choose light excitation with a particular helicity (σ^+) to selectively excite a particular valley (K). Shown in Figure 2a,b, we found that, even at the absence of an external magnetic field (blue curve in Figure 2b), the photocurrent response exhibits a resonance response at a few particular excitation photon energies. The most pronounced one is at 1.730 eV, the same as the absorption resonance of the 1s state of the A exciton in WSe_2 (see Supporting Information 2). The second pronounced resonance peak is located at 1.861 eV, which we assign as the 2s state of the A exciton due to the agreement with the absorption spectra (Supporting Information 2). There is a third peak smaller in magnitude but clearly visible at 1.880 eV, which we will show in the following discussion to be the 3s state of the A exciton. As we increase the magnitude of the out-of-plane magnetic field, it is evident from Figure 2b that the resonance at 3s is enhanced at a magnetic field of 15 T (−15 T), with an even higher-order excited exciton state, up to 8s, being visible at 4.2 K. The detailed photocurrent spectra as a function of the out-of-plane magnetic field is shown in Figure 2a, with all the resonance peaks (bright line) exhibiting distinctive dependence on the magnetic field. These dependences, as we show below, are consistent with the expected absorption resonance for different exciton states, from 1s to 8s. We note that the photocurrent spectra are taken at the zero gate voltage, when the WSe_2 is charge neutral. As soon as we change the gate voltage to the electron or hole dope the WSe_2, all the resonance peaks disappear quickly (see Supporting Information 10 for details).

III. MAGNETIC-FIELD DEPENDENCE OF RYDBERG EXCITON RESONANCE

We then use optical excitation with different helicities to access the photocurrent spectra of K and K′ valleys, mainly focusing

https://dx.doi.org/10.1021/acs.nanolett.0c03167
Nano Lett. 2020, 20, 7635−7641

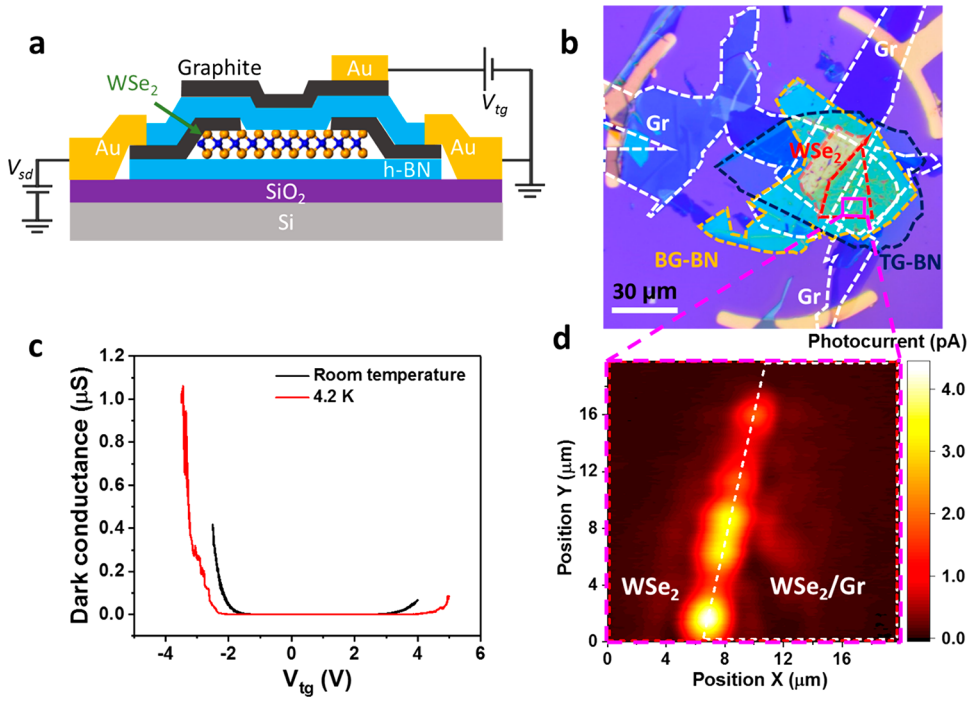

Figure 1. Photocurrent response from BN encapsulated monolayer WSe_2 device. (a) Schematic of the BN encapsulated monolayer WSe_2 device. Two pieces of few-layer graphene are used as the source and drain electrodes, and one piece of few-layer graphene is used as the top gate electrode, with the top BN layer working as the gate dielectric. (b) Optical microscope image of the device. (c) Source-drain current of the WSe_2 device as a function of the top gate voltage, with the applied bias of 100 mV, at room temperature (black line) and 4.2 K (red line). (d) Spatially resolved photocurrent image of the boxed region in (b), with the CW excitation centered at 1.959 eV and excitation power of 1 μW. The color represents the photocurrent magnitude. The red and white dash line outlines the boundary of the WSe_2 and few-layer graphene electrode, respectively. The few-layer graphene electrode on the right is on top of the monolayer WSe_2 and is denoted as WSe_2/Gr.

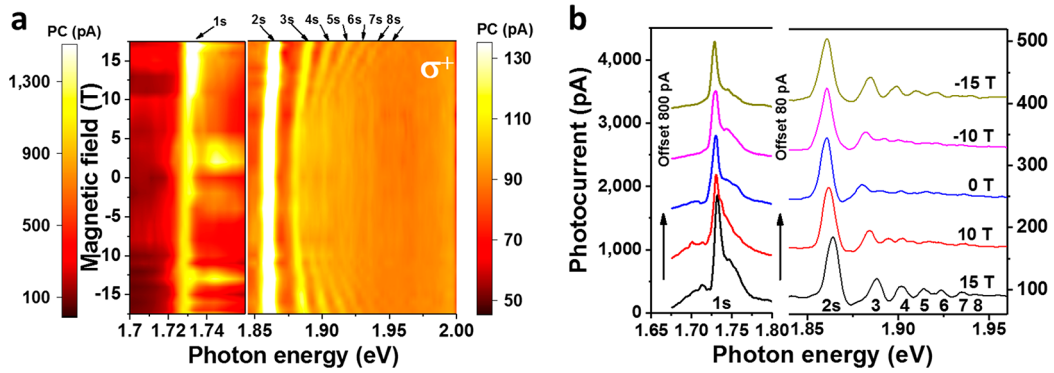

Figure 2. Photocurrent spectroscopy of exciton Rydberg series in BN encapsulated monolayer WSe_2. (a) Photocurrent response of the monolayer WSe_2 device as a function of the excitation photon energy and magnetic field for the σ^+ photoexcitation (K valley). The color represents the photocurrent magnitude, which is most pronounced as the excitation photon energy is in resonance with the 1s state (1.725 eV) of the A exciton of monolayer WSe_2. The resonance corresponding to the Rydberg series from 2s to 8s is clearly visible on the right. (b) Photocurrent response as a function of the excitation photon energy for the different magnetic fields. All the measurements are taken with 100 mV bias voltage and a temperature of 4.2 K.

on the exciton excited state starting from 2s. We normalize the photocurrent with the excitation laser power, and the normalized photoresponsivity spectra were further background-subtracted and shown in Figure 3a,b. It is evident from Figure 3a,b that, starting from 3s, the resonance peak position is approximately a quadratic function of the magnitude of the magnetic-field B, significantly different from the 2s. This distinct difference of the magnetic field can be understood by considering the energy shift of Rydberg (ns) exciton in the presence of the magnetic field.[9−12] In the low-magnetic-field limit where Landau quantization does not need to be considered, the resonance energy for each ns exciton state can be expressed as a function of the magnetic field as

$$E_{ns} = E_{ns}^{0} + \frac{1}{2}\sigma g \mu_B B + \Delta E_{dm} \quad (1)$$

where E_{ns}^{0} is the energy of the ns state at zero magnetic field, σ is the valley index that is +1 for the K valley and −1 for the K′ valley, μ_B is the value of Bohr magneton, and g is the Landé g-factor. The third term ΔE_{dm} is the diamagnetic shift. In the low-magnetic-field limit, where the cyclotron resonance energy

https://dx.doi.org/10.1021/acs.nanolett.0c03167
Nano Lett. 2020, 20, 7635−7641

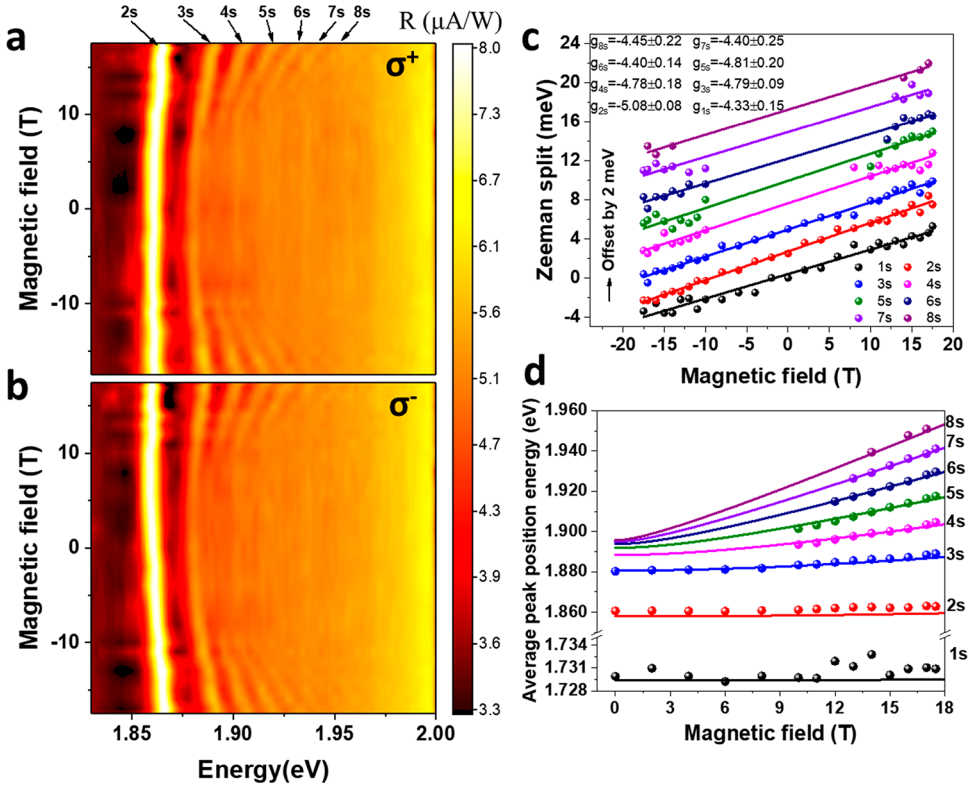

Figure 3. Photocurrent spectroscopy of exciton Rydberg series from the K and K′ valleys. (a) and (b) are the photocurrent responsivity of the monolayer WSe_2 device as a function of the excitation photon energy and the magnetic field for the K (a) and K′ valley (b). Background of photocurrent is subtracted in (a) and (b) for better illustration (see Supporting Information 7 for details). (c) Difference of the peak energy for different Rydberg excited states (Zeeman splitting) as a function of the magnetic field. (d) Average of the peak energy for different Rydberg excited states at the K and K′ valleys (Zeeman splitting) as a function of the magnetic field. The solid dots are extracted from experimental data, and the solid lines are from theoretical fittings. All the measurements are taken with a bias voltage of 100 mV and a temperature of 4.2 K.

$\hbar\omega_B = \frac{e\hbar}{m_r}|B|$ is much smaller than the exciton binding energy, the diamagnetic shift ΔE_{dm} can be expressed as $\frac{e^2}{8m_r}\langle r^2\rangle_{ns}B^2$, with m_r being the reduced mass of exciton and $\langle r^2\rangle_{ns}$ being the square of the expected *ns* exciton radius. For ground-state 1s, as the exciton is strongly bounded, $\langle r^2\rangle_{1s}$ is small, and the energy shift $\Delta E = E_{ns} - E^0_{ns}$ is dominated by the valley-Zeeman term that linearly depends on the magnetic field. Even for the 2s state, the linear term is still more significant (Figure 3a,b). In contrast, for the higher-order excited state starting from 3s, $\langle r^2\rangle_{ns}$ increases significantly, and the diamagnetic shift term will dominate. Therefore, the exciton energy shift will be an approximately quadratic function of the magnetic field. The distinctive difference in the magnetic-field dependence for different ns states is evident in Figure 3a,b.

In the extremely high-magnetic-field limit, though, the Landau levels (LLs) will form. If $\frac{e\hbar}{m_r}|B|$ is much larger than the binding energy, and the absorption is dominated by the inter-LL transitions, which is valley-selective due to the nontrivial Berry phase.[25−29] The diamagnetic shift term ΔE_{dm} will be $(n - \frac{1}{2})\frac{e\hbar}{m_r}|B|$, where n is the number of allowed inter-LL transitions for each valley. As a result, the energy shift $\Delta E = E_{ns} - E^0_{ns}$ will again be a linear function of the magnetic field in the high-field limit.[14−16] We note here that, as the binding energy of the high-order excited state decreases, the high-field limit can be easier to achieve for the ns state when $n \gg 1$. We will discuss this further later with our data from the high-order excited state.

Eq 1 allows us to quantitatively analyze the experimental data. From the photocurrent spectra of the K and K′ valleys (Figure 3a,b), the energy difference of the resonance peaks $\Delta E = E_{ns} - E^0_{ns}$ is given by the expression of $\frac{1}{2}g\mu_B B$, which is the valley-Zeeman shift for different excited exciton states. Therefore, we extract the energy difference of the resonance for the K (Figure 3a) and K′ valleys (Figure 3b) for the exciton with the same principal number (n), and we plot it as the function of the magnetic field as shown in Figure 3c. We can see that the resonance energy difference up to 8s can all be well fitted with a linear fitting, which gives a *g*-factor between 4 to 5. The *g*-factor of the A exciton has been reported to be in this range for excited states up to 5s.[15,16] Here, we show that the *g*-factor value of the 8s is also similar. This insensitive dependence of the *g*-factor on the quantum principal number suggests that the Zeeman shift of the exciton mainly originates from the Zeeman shift of the band edges.

IV. FITTING WITH NUMERICAL CALCULATION

Also, from eq 1, the average energy of the resonance peaks from the photocurrent spectra of the K and K′ valleys, $\bar{E}_{ns} = \frac{1}{2}(E_K + E_{K'})$, can be expressed as $E^0_{ns} + \Delta E_{dm}$, noting that ΔE_{dm} is an even function of the magnetic field, and the valley-Zeeman shift from K or K′ valleys is an odd function of the magnetic field that cancels each other. As a result, the shift of the average resonance energy for ns, $\Delta\bar{E}_{ns} = \bar{E}_{ns} - E^0_{ns}$, will

https://dx.doi.org/10.1021/acs.nanolett.0c03167
Nano Lett. 2020, 20, 7635−7641

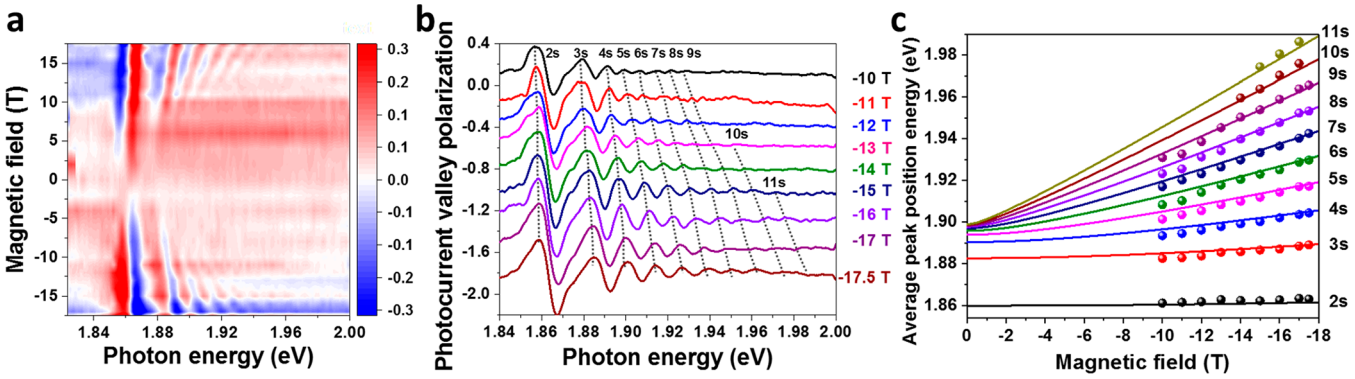

Figure 4. Photocurrent spectroscopy of valley polarization for exciton Rydberg series of monolayer WSe_2. (a) Color plot of the photocurrent valley polarization, defined as $\frac{PC_K - PC_{K'}}{PC_K + PC_{K'}}$, as a function of the excitation photon energy and magnetic field. (b) Line traces of photocurrent valley polarization for different magnetic fields. The dashed lines are the eye guide to track the peaks associated with different Rydberg excited states up to 11s. (c) The energy position of the node in (a), where the photocurrent valley polarization is zero, as a function of the magnetic field. The solid dots are extracted experimental data, and the solid lines are from the numerical calculations.

only be determined by the diamagnetic shift, and the experimentally extracted value is shown in Figure 3d (solid dots).

For most of our data, we are dealing with the scenario that the strong Coulomb interaction and Landau quantization coexist, which gives rise to the intriguing question of the exciton behavior in a strong quantizing magnetic field. Since neither the Coulomb interaction or the Landau quantization energy can be treated as a perturbation, we do not have an analytical solution. Instead, we can numerically calculate average resonance shift $\Delta\bar{E}_{ns}$ as a function of the magnetic field. Here, we adopt a nonhydrogenic screened Keldysh potential,[16,30−32] which is given by

$$V(r) = -\frac{e^2}{8\varepsilon_0 r_0}\left[H_0\left(\frac{\varepsilon r}{r_0}\right) - Y_0\left(\frac{\varepsilon r}{r_0}\right)\right]$$

where $\varepsilon = (\varepsilon_{top} + \varepsilon_{bottom})/2$ is the averaged relative dielectric constant of the surroundings, ε_0 is the vacuum permittivity, and $r_0 = 2\pi\chi_{2D}$ is the screening length with χ_{2D} being the 2D polarizability. H_0 and Y_0 are the Struve and Bessel functions of the second kind, respectively. The numerically calculated $\Delta\bar{E}_{ns}$ as a function of the magnetic field is best fitted with our experimental data with the fitting parameters $\varepsilon = 4.3$, $r_0 = 4.5$ nm, and $m_r = 0.2m_0$, where m_0 is the free electron mass in a vacuum (see Supporting Information 5 for details). Figure 3d shows that the numerical calculation is in excellent agreement with the experimental data for the exciton state from 2s to 8s. The fitting parameter, screening length $r_0 = 4.5$ nm, is consistent with the theory[33,34] and previous experimental work.[15] Our obtained fitting result of the BN dielectric constant, $\varepsilon = 4.3$, is consistent with previous infrared measurements.[35]

V. DISCUSSION AND PHOTOCURRENT VALLEY POLARIZATION

It is worth noting that even higher-order exciton excited states ($n > 8$) are also vaguely visible in the color plots (Figure 3a,b), especially for the magnetic field near −17 T. To extract this information out, we exploit the valley degrees of freedom to better subtract the background.

As we can see from eq 1, the valley degrees of freedom helps lift the energy degeneracy of the exciton states at the K and K′ valleys. Hence, we define the valley polarization of the photocurrent as $P_{PC} = \frac{PC_K - PC_{K'}}{PC_K + PC_{K'}}$, where PC_K ($PC_{K'}$) is the photocurrent response from the K (K′) valley. If the separation of the resonances from the K and K′ valleys is much larger than the line width of the resonance, the photocurrent valley polarization, P_{PC}, will have an extreme value of 50% for the K valley resonance and −50% valley resonance. In reality, the line width broadens for the higher-order excited states, and the peak value of the photocurrent valley polarization becomes smaller, but we can still use the positive or negative peak to track the shift of the resonance of the K and K′ valleys (see Supporting Information 4 for details).

The experimentally extracted valley polarization as a function of the magnetic field can be found in the color plot of Figure 4a. It is evident that higher excited exciton state with the principal number $n > 8$ is visible, especially for the magnetic field <−15 T. The valley polarization for different negative magnetic fields from −10 to −17.5 T can also be found in the line traces shown in Figure 4b (line traces for other magnetic fields can be found in Supporting Information 4), which shows that we can identify the excited exciton states up to 11s. The average resonance energy, which corresponds to the node of zero photocurrent valley polarization, is in excellent agreement with the numerical calculation, as shown in Figure 4c, with the fitting parameters obtained in the previous discussion ($\varepsilon = 4.3$, $r_0 = 4.5$ nm, and $m_r = 0.2m_0$). We can thus obtain the binding energy and radius extension for all the excited exciton states up to 11s (Table 1), which is the most comprehensive study of the Rydberg exciton in TMDC up to date. It is worth noting that the binding energy of 11s exciton (1.2 meV) is significantly smaller than the Landau quantization energy $\hbar\omega_B = \frac{e\hbar}{m_r}|B|$ at 15 T (~8.69 meV), which suggests that we are in the high-magnetic-field limit. Per our previous discussion, in the high-field limit, the average energy shift will be a linear function of the B field, with the slope asymptotically approaching $(n - \frac{1}{2})\frac{e\hbar}{m_r}$. Therefore, we could obtain the reduced mass of the exciton solely from experimental data. Fitting all Rydberg exciton data shows that, starting from 9s, we reach a saturating reduced mass of $0.2m_0$ (see Supporting Information 8 and 9 for details), in excellent agreement with fitting result mentioned above,

https://dx.doi.org/10.1021/acs.nanolett.0c03167
Nano Lett. 2020, 20, 7635−7641

confirming that we are in the high-field limit for $n \geq 9$ excitons even with a magnetic field as low as ~10 T. Monolayer WSe_2, therefore, provides an intriguing platform to investigate the different interplay between the Coulomb interaction and Landau quantization. By tuning the principal number n of Rydberg excitons, we can smoothly transition from a low to high-magnetic-field limit with a reasonable magnetic field between 10 to 17 T, which is drastically advantageous for detailed investigations considering the extremely strong magnetic field (~91 T) needed in the previous study.[14] Finally, these giant valley-polarized Rydberg excitons in monolayer WSe_2 set up the stage to the future investigation of the greatly enhanced exciton−exciton interaction in two dimensions.

■ ASSOCIATED CONTENT

Supporting Information

The Supporting Information is available free of charge at https://pubs.acs.org/doi/10.1021/acs.nanolett.0c03167.

Details about sample preparation, optical characterization and data analysis (PDF)

■ AUTHOR INFORMATION

Corresponding Author

Su-Fei Shi − *Department of Chemical and Biological Engineering and Department of Electrical, Computer & Systems Engineering, Rensselaer Polytechnic Institute, Troy, New York 12180, United States;* orcid.org/0000-0001-5158-805X; Email: shis2@rpi.edu

Authors

Tianmeng Wang − *Department of Chemical and Biological Engineering, Rensselaer Polytechnic Institute, Troy, New York 12180, United States;* orcid.org/0000-0001-7399-7671

Zhipeng Li − *Department of Chemical and Biological Engineering, Rensselaer Polytechnic Institute, Troy, New York 12180, United States;* orcid.org/0000-0003-1115-1077

Yunmei Li − *Department of Physics, The University of Texas at Dallas, Richardson, Texas 75080, United States*

Zhengguang Lu − *National High Magnetic Field Lab, Tallahassee, Florida 32310, United States; Department of Physics, Florida State University, Tallahassee, Florida 32306, United States*

Shengnan Miao − *Department of Chemical and Biological Engineering, Rensselaer Polytechnic Institute, Troy, New York 12180, United States*

Zhen Lian − *Department of Chemical and Biological Engineering, Rensselaer Polytechnic Institute, Troy, New York 12180, United States*

Yuze Meng − *Department of Chemical and Biological Engineering, Rensselaer Polytechnic Institute, Troy, New York 12180, United States*

Mark Blei − *School for Engineering of Matter, Transport and Energy, Arizona State University, Tempe, Arizona 85287, United States*

Takashi Taniguchi − *Research Center for Functional Materials, National Institute for Materials Science, Tsukuba 305-0044, Japan;* orcid.org/0000-0002-1467-3105

Kenji Watanabe − *International Center for Materials Nanoarchitectonics, National Institute for Materials Science, Tsukuba 305-0044, Japan;* orcid.org/0000-0003-3701-8119

Sefaattin Tongay − *School for Engineering of Matter, Transport and Energy, Arizona State University, Tempe, Arizona 85287, United States;* orcid.org/0000-0001-8294-984X

Dmitry Smirnov − *National High Magnetic Field Lab, Tallahassee, Florida 32310, United States;* orcid.org/0000-0001-6358-3221

Chuanwei Zhang − *Department of Physics, The University of Texas at Dallas, Richardson, Texas 75080, United States*

Complete contact information is available at: https://pubs.acs.org/10.1021/acs.nanolett.0c03167

Author Contributions

◆T.W., Z. Li, Y.L., and Z. Lu contributed equally to this work.

Author Contributions

S.-F.S. conceived the experiment and supervised the project. Z. Li, T.W., Y.M., and Z. Lian fabricated the devices. T.W., Z. Li, and Z. Lu performed the measurements. S.-F.S., T.W., S.M., and Z. Li analyzed the data. S.-F.S., T.W., Y.L., and C.Z. developed the theoretical understanding. T.T. and K.W. grew the BN crystals. S.T. and M.B. grew high-purity WSe_2 crystals through the flux zone growth technique. D.S. supervised the magneto-PL measurements. S.-F.S. wrote the manuscript with input from all the other coauthors. All authors discussed the results and contributed to the manuscript.

Notes

The authors declare no competing financial interest.

The data that support the findings of this study are available from the authors on reasonable request; see author contributions for specific data sets.

■ ACKNOWLEDGMENTS

This work is primarily supported by AFOSR through Grant FA9550-18-1-0312. T.W. and S.-F.S. acknowledge support from ACS PRF through Grant 59957-DNI10. Z. Lian and S.-F.S. acknowledge support from NYSTAR through Focus Center-NY−RPI Contract C150117. The device fabrication was supported by the Micro and Nanofabrication Clean Room (MNCR) at Rensselaer Polytechnic Institute (RPI). S.T. acknowledges support from NSF DMR-1904716, DMR-1838443, CMMI-1933214, and DOE-SC0020653. K.W. and T.T. acknowledge support from the Elemental Strategy Initiative conducted by the MEXT, Japan, Grant Number JPMXP0112101001, JSPS KAKENHI Grant Numbers JP20H00354 and the CREST(JPMJCR15F3), JST. Z. Lu and D.S. acknowledge support from the US Department of Energy (DE-FG02-07ER46451) for magneto-photoluminescence measurements performed at the National High Magnetic Field Laboratory, which is supported by National Science Foundation through NSF/DMR-1644779 and the State of Florida. Y.L. and C.Z. are supported by AFOSR (Grant No. FA9550-16-1-0387), NSF (Grant No. PHY-1806227), and ARO (Grant No. W911NF-17-1-0128). S.-F.S. also acknowledges the support from NSF through Career Award DMR-1945420.

■ REFERENCES

(1) Gallagher, T. F. Rydberg Atoms. *Rep. Prog. Phys.* **1988**, *51*, 143−188.

(2) Browaeys, A.; Lahaye, T. Many-Body Physics with Individually Controlled Rydberg Atoms. *Nat. Phys.* **2020**, *16*, 132−142.

(3) Chernikov, A.; Berkelbach, T. C.; Hill, H. M.; Rigosi, A.; Li, Y.; Aslan, O. B.; Reichman, D. R.; Hybertsen, M. S.; Heinz, T. F. Exciton

Binding Energy and Nonhydrogenic Rydberg Series in Monolayer WS_2. *Phys. Rev. Lett.* **2014**, *113*, 076802.
(4) He, K.; Kumar, N.; Zhao, L.; Wang, Z.; Mak, K. F.; Zhao, H.; Shan, J. Tightly Bound Excitons in Monolayer WSe_2. *Phys. Rev. Lett.* **2014**, *113*, 026803.
(5) Chernikov, A.; Van Der Zande, A. M.; Hill, H. M.; Rigosi, A. F.; Velauthapillai, A.; Hone, J.; Heinz, T. F. Electrical Tuning of Exciton Binding Energies in Monolayer WS2. *Phys. Rev. Lett.* **2015**, *115*, 126802.
(6) Butscher, B.; Nipper, J.; Balewski, J. B.; Kukota, L.; Bendkowsky, V.; Löw, R.; Pfau, T. Atom-Molecule Coherence for Ultralong-Range Rydberg Dimers. *Nat. Phys.* **2010**, *6*, 970−974.
(7) Madjarov, I. S.; Covey, J. P.; Shaw, A. L.; Choi, J.; Kale, A.; Cooper, A.; Pichler, H.; Schkolnik, V.; Williams, J. R.; Endres, M. High-Fidelity Entanglement and Detection of Alkaline-Earth Rydberg Atoms. *Nat. Phys.* **2020**, *16*, 857.
(8) Saffman, M.; Walker, T. G.; Mølmer, K. Quantum Information with Rydberg Atoms. *Rev. Mod. Phys.* **2010**, *82*, 2313−2363.
(9) Kazimierczuk, T.; Fröhlich, D.; Scheel, S.; Stolz, H.; Bayer, M. Giant Rydberg Excitons in the Copper Oxide Cu_2O. *Nature* **2014**, *514*, 343−347.
(10) Faure, S.; Guillet, T.; Lefebvre, P.; Bretagnon, T.; Gil, B. Comparison of Strong Coupling Regimes in Bulk GaAs, GaN, and ZnO Semiconductor Microcavities. *Phys. Rev. B: Condens. Matter Mater. Phys.* **2008**, *78*, 235323.
(11) Jadczak, J.; Kutrowska-Girzycka, J.; Smoleński, T.; Kossacki, P.; Huang, Y. S.; Bryja, L. Exciton Binding Energy and Hydrogenic Rydberg Series in Layered ReS_2. *Sci. Rep.* **2019**, *9*, 1578.
(12) Matsumoto, H.; Saito, K.; Hasuo, M.; Kono, S.; Nagasawa, N. Revived Interest on Yellow-Exciton Series in Cu_2O: An Experimental Aspect. *Solid State Commun.* **1996**, *97*, 125−129.
(13) Xu, X.; Yao, W.; Xiao, D.; Heinz, T. F. Spin and Pseudospins in Layered Transition Metal Dichalcogenides. *Nat. Phys.* **2014**, *10*, 343.
(14) Goryca, M.; Li, J.; Stier, A. V.; Taniguchi, T.; Watanabe, K.; Courtade, E.; Shree, S.; Robert, C.; Urbaszek, B.; Marie, X.; et al. Revealing Exciton Masses and Dielectric Properties of Monolayer Semiconductors with High Magnetic Fields. *Nat. Commun.* **2019**, *10*, 4172.
(15) Stier, A. V.; Wilson, N. P.; Clark, G.; Xu, X.; Crooker, S. A. Probing the Influence of Dielectric Environment on Excitons in Monolayer WSe2: Insight from High Magnetic Fields. *Nano Lett.* **2016**, *16*, 7054−7060.
(16) Stier, A. V.; Wilson, N. P.; Velizhanin, K. A.; Kono, J.; Xu, X.; Crooker, S. A. Magnetooptics of Exciton Rydberg States in a Monolayer Semiconductor. *Phys. Rev. Lett.* **2018**, *120*, 057405.
(17) Massicotte, M.; Vialla, F.; Schmidt, P.; Lundeberg, M. B.; Latini, S.; Haastrup, S.; Danovich, M.; Davydovskaya, D.; Watanabe, K.; Taniguchi, T.; et al. Dissociation of Two-Dimensional Excitons in Monolayer WSe_2. *Nat. Commun.* **2018**, *9*, 1633.
(18) Molas, M. R.; Slobodeniuk, A. O.; Nogajewski, K.; Bartos, M.; Bala; Babiński, A.; Watanabe, K.; Taniguchi, T.; Faugeras, C.; Potemski, M. Energy Spectrum of Two-Dimensional Excitons in a Nonuniform Dielectric Medium. *Phys. Rev. Lett.* **2019**, *123*, 136801.
(19) Li, Z.; Wang, T.; Lu, Z.; Jin, C.; Chen, Y.; Meng, Y.; Lian, Z.; Taniguchi, T.; Watanabe, K.; Zhang, S.; et al. Revealing the Biexciton and Trion-Exciton Complexes in BN Encapsulated WSe_2. *Nat. Commun.* **2018**, *9*, 3719.
(20) Li, Z.; Wang, T.; Jin, C.; Lu, Z.; Lian, Z.; Meng, Y.; Blei, M.; Gao, S.; Taniguchi, T.; Watanabe, K.; et al. Emerging Photoluminescence from the Dark-Exciton Phonon Replica in Monolayer WSe_2. *Nat. Commun.* **2019**, *10*, 2469.
(21) Li, Z.; Wang, T.; Lu, Z.; Khatoniar, M.; Lian, Z.; Meng, Y.; Blei, M.; Taniguchi, T.; Watanabe, K.; McGill, S. A.; et al. Direct Observation of Gate-Tunable Dark Trions in Monolayer WSe_2. *Nano Lett.* **2019**, *19*, 6886−6893.
(22) Quereda, J.; Ghiasi, T. S.; You, J. S.; van den Brink, J.; van Wees, B. J.; van der Wal, C. H. Symmetry Regimes for Circular Photocurrents in Monolayer $MoSe_2$. *Nat. Commun.* **2018**, *9*, 3346.
(23) Klots, A. R.; Newaz, A. K. M.; Wang, B.; Prasai, D.; Krzyzanowska, H.; Lin, J.; Caudel, D.; Ghimire, N. J.; Yan, J.; Ivanov, B. L.; et al. Probing Excitonic States in Suspended Two-Dimensional Semiconductors by Photocurrent Spectroscopy. *Sci. Rep.* **2015**, *4*, 6608.
(24) Massicotte, M.; Schmidt, P.; Vialla, F.; Schädler, K. G.; Reserbat-Plantey, a.; Watanabe, K.; Taniguchi, T.; Tielrooij, K. J.; Koppens, F. H. L. Picosecond Photoresponse in van Der Waals Heterostructures. *Nat. Nanotechnol.* **2016**, *11*, 42.
(25) Wang, Z.; Shan, J.; Mak, K. F. Valley- and Spin-Polarized Landau Levels in Monolayer WSe_2. *Nat. Nanotechnol.* **2017**, *12*, 144−149.
(26) Chu, R.-L.; Li, X.; Wu, S.; Niu, Q.; Yao, W.; Xu, X.; Zhang, C. Valley-Splitting and Valley-Dependent Inter-Landau-Level Optical Transitions in Monolayer MoS_2 Quantum Hall Systems. *Phys. Rev. B: Condens. Matter Mater. Phys.* **2014**, *90*, 045427.
(27) Cai, T.; Yang, S. A.; Li, X.; Zhang, F.; Shi, J.; Yao, W.; Niu, Q. Magnetic Control of the Valley Degree of Freedom of Massive Dirac Fermions with Application to Transition Metal Dichalcogenides. *Phys. Rev. B: Condens. Matter Mater. Phys.* **2013**, *88*, 115140.
(28) Rose, F.; Goerbig, M. O.; Piéchon, F. Spin- and Valley-Dependent Magneto-Optical Properties of MoS_2. *Phys. Rev. B: Condens. Matter Mater. Phys.* **2013**, *88*, 125438.
(29) Wang, T.; Li, Z.; Lu, Z.; Li, Y.; Miao, S.; Lian, Z.; Meng, Y.; Blei, M.; Taniguchi, T.; Watanabe, K.; et al. Observation of Quantized Exciton Energies in Monolayer WSe_2 under a Strong Magnetic Field. *Phys. Rev. X* **2020**, *10*, 021024.
(30) Keldysh, L. Coulomb Interaction in Thin Semiconductor and Semimetal Films. *JETP Letters* **1979**, *29*, 658−661.
(31) Kidd, D. W.; Zhang, D. K.; Varga, K. Binding Energies and Structures of Two-Dimensional Excitonic Complexes in Transition Metal Dichalcogenides. *Phys. Rev. B* **2016**, *93*, 125423.
(32) Mostaani, E.; Szyniszewski, M.; Price, C. H.; Maezono, R.; Danovich, M.; Hunt, R. J.; Drummond, N. D.; Fal'Ko, V. I. Diffusion Quantum Monte Carlo Study of Excitonic Complexes in Two-Dimensional Transition-Metal Dichalcogenides. *Phys. Rev. B: Condens. Matter Mater. Phys.* **2017**, *96*, 075431.
(33) Kylänpää, I.; Komsa, H.-P. Binding Energies of Exciton Complexes in Transition Metal Dichalcogenide Monolayers and Effect of Dielectric Environment. *Phys. Rev. B: Condens. Matter Mater. Phys.* **2015**, *92*, 205418.
(34) Berkelbach, T. C.; Hybertsen, M. S.; Reichman, D. R. Theory of Neutral and Charged Excitons in Monolayer Transition Metal Dichalcogenides. *Phys. Rev. B: Condens. Matter Mater. Phys.* **2013**, *88*, 045318.
(35) Geick, R.; Perry, C. H.; Rupprecht, G. Normal Modes in Hexagonal Boron Nitride. *Phys. Rev.* **1966**, *146* (2), 543−547.

https://dx.doi.org/10.1021/acs.nanolett.0c03167
Nano Lett. 2020, 20, 7635−7641